Turkish Journal of Electrical Engineering & Computer Sciences

http://journals.tubitak.gov.tr/elektrik/

Research Article

Turk J Elec Eng & Comp Sci
(2021) 29: 421 – 436

doi:10.3906/elk-1907-15

Neurofuzzy robust backstepping based MPPT control for photovoltaic system

Kamran ALI[1,*], **Laiq KHAN**[1], **Qudrat KHAN**[2], **Shafaat ULLAH**[1], **Naghmash ALI**[3]
[1]Department of Electrical and Computer Engineering, COMSATS University Islamabad, Pakistan
[2]Center for Advanced Studies in Telecommunication, COMSATS University Islamabad, Pakistan
[3]School of Electrical Engineering, Shandong University, China

Received: 02.07.2019 • **Accepted/Published Online:** 06.02.2020 • **Final Version:** 27.01.2021

Abstract: Linear maximum power point tracking (MPPT) techniques are unable to achieve the desired performance and efficiency under wide variation in atmospheric conditions (temperature and irradiance) and consequently the maximum power point (MPP). Hence, the design and implementation of a nonlinear MPPT controller is essential to address the problems associated with the variations of the MPP. In this research article, a new nonlinear robust backstepping-based MPPT control technique is proposed for a standalone PV array connected to a dynamic load, and its performance comparison with existing backstepping, integral backstepping and conventional proportional integral derivative (PID) and perturb and observe (P&O) based MPPT techniques is provided. Simulations, performed in Matlab/Simulink platform, verify the effectiveness of the proposed MPPT technique and demonstrate its superior performance to the backstepping, integral backstepping and conventional MPPT techniques under simultaneous variation in irradiance and temperature and certain faults occurring in the system.

Key words: Photovoltaic (PV), maximum power point tracking (MPPT), buck-boost converter, robust backstepping (RB), Neurofuzzy estimator

1. Introduction

Solar energy finds its place among the most reliable and efficient energy sources. It is a clean and pollution-free energy source fascinating the interest of researchers for harnessing solar energy through PV (photovoltaic) modules [1].

The output power versus voltage ($P-V$) characteristics of a PV system, being nonlinear, exhibits a unique maximum, called the maximum power point (MPP). This MPP lies at the knee of the ($P-V$) curve. Since, power output of the PV system varies with varying atmospheric conditions (temperature and irradiance), it is essential to continuously track the MPP for the maximum power extraction from the PV system, under varying ambient conditions [2]. Different maximum power point tracking (MPPT) techniques are employed to track the MPP of the PV system for extracting maximum power and enhance the conversion efficiency [3].
The switching functions of the converter along with the electrical characteristics ($P-V$ and $I-V$) of a PV system are nonlinear. Therefore, stable operation of the PV systems under varying environmental conditions is a challenging task. Under such circumstances, linear MPPT controllers are unable to achieve the desired MPPT performance under wide variation in environmental conditions [4]. Hence, the design and implementation of a nonlinear MPPT controller is essential to address the problems associated with the variations of the maximum

*Correspondence: kamran_ciit33@yahoo.com

power point.

There are several nonlinear MPPT control techniques, such as sliding mode controller (SMC) [5], feedback linearizing controller (FBLC) [6], and model predictive controller (MPC) [7]. Among these nonlinear techniques, FBLC has been frequently employed for nonlinear controller design, which transforms a given nonlinear system into a partially/fully equivalent linear system after canceling the nonlinearities. However, it needs the exact parameters of the nonlinear system for its implementation. Moreover, during this linearization process, often some useful inherent nonlinearity within the system also gets cancelled [6]. The complete cancelation of useful nonlinear system dynamics in FBLC can be avoided and stabilized by employing a nonlinear backstepping controller [8]. The SMC has low sensitivity to external disturbances and parameters variation. However, the construction of a time-varying sliding surface is a quite difficult task [9]. An MPC requires exact system parameters for its successful implementation [7].

In [10] and [11], nonlinear Lyapunov stability theory based backstepping and integral backstepping based MPPT techniques have been proposed, respectively, for a PV array connected to a purely resistive load. Both the stated strategies have been shown to perform well either under varying temperature alone, or varying irradiance alone, but not both. Similarly, the performance of the stated techniques have not been tested against simultaneous variation in temperature and irradiance and certain faults occurring in the system.

The backstepping is a recursive control design strategy. The principal idea is the stabilization of the virtual control state [12, 13]. It is based on designing an MPPT controller recursively by choosing some of the system state variables as the virtual controllers, and then designing intermediate control laws for each of the selected virtual controller. This approach is well-suitable for boundary control problems. While the control is acting only from the boundary, its main feature is the capability of cancelling out all the destabilizing effects (i.e. forces or terms) appearing throughout the domain. Its attractive features include: fast dynamic response, robustness to system parametric uncertainties, good performance against unmodelled system dynamics and external disturbance rejection [14, 15].

To counteract the aforementioned shortcomings in [10, 11], a hybrid nonlinear robust backstepping based MPPT technique is proposed in this research article. The proposed technique is tested on a standalone PV system comprising a PV array, a non-inverting DC-DC buck-boost power converter, a resistive load (lighting and electric fans) as well as a dynamic load (sound system used in military parade grounds, large religious gatherings and holy worship places). Its performance comparison with existing backstepping, integral backstepping and conventional PID and P&O based MPPT techniques is provided. Simulations are performed in Matlab/Simulink, under simultaneous variation in temperature and irradiance and multiple faults occuring in the system, to verify the effectiveness and superior performance of the proposed MPPT technique.

The present research article is organized as follows: Section 2 presents the NeuroFuzzy estimator. The overall system modelling is given in Section 3. Section 4 is dedicated to the proposed control system design. The effectiveness of the proposed MPPT control system is validated in Section 5. Finally, conclusion is drawn in Section 6.

2. Reference peak power voltage generation

The reference peak power voltage, V_{MPP} or v_{ref} is generated through a NeuroFuzzy network [16]. This network is based on Takagi-Sugeno-Kang (TSK) fuzzy inference system as illustrated in Figure 1. It takes 2 inputs (temperature and irradiance) and estimates the output (V_{MPP}). Its input layer is the fuzzification

layer with 3 Gaussian membership functions for each input variable. Whereas, its output layer consists of a linear equation for each rule. The reference peak power voltage, under varying irradiance, S (W/m^2), and temperature T (^oC), is depicted in Figure 1(a) by a 3D-plane.

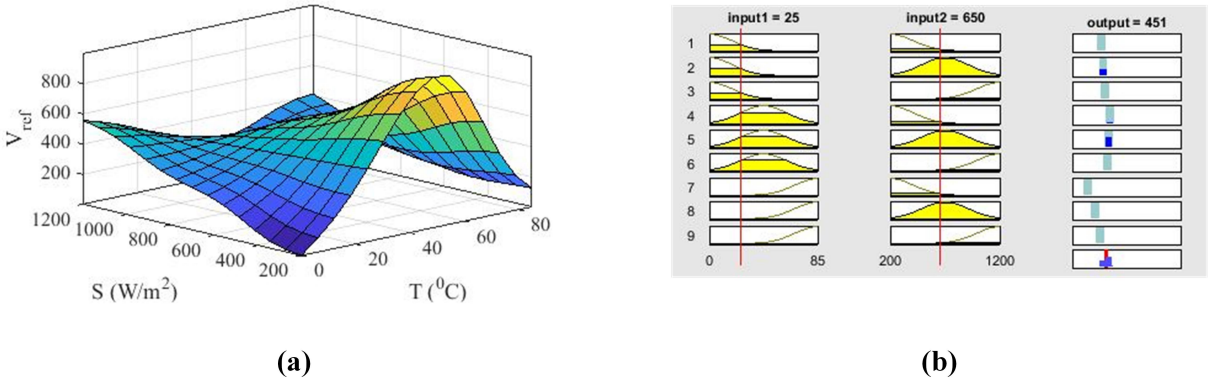

(a) **(b)**

Figure 1. NeuroFuzzy estimator (a) 3-D plot (b) rule-base.

3. System modelling

In this section, state-space modelling of the sound system, PV module, and DC-DC converter are described in detail.

3.1. Mathematical modelling of PV module

In order to design an efficient PV system, a reliable and accurate solar cell modelling is essential. The PV cell is an electrical device, which uses the photovoltaic effect to convert the solar energy directly into electrical energy. The PV module is composed of a group of PV cells which are joined in series and/or parallel to generate higher power, voltage, and current levels. The energy produced from PV system depends on temperature, solar irradiation, the dirt, shaded condition and the PV module output voltage, etc. In the literature, 2 types of PV cell modelling are presented: (1) Single-diode model and (2) 2-diode model. The 2-diode model is reliable and accurate than the single-diode model, but it involves more parameters to model an accurate PV, thus making it a complex choice. Therefore, in this research article the authors have used the single-diode model for simplicity, reasonable accuracy, and less complexity as illustrated in Figure 2.

The output current of a PV cell, based on the single-diode model is given in the following equation [17]:

$$I_o = N_p I_{ph} - N_p I_{rs}\left[\exp\left(\frac{q(v + R_s I_o)}{AkTN_s}\right) - 1\right] - N_p\left(\frac{q(v + R_s I_o)}{N_s R_{sh}}\right) \quad (1)$$

Where, I_o is the PV cell output current, I_{rs} is the reverse saturation current of the PV cell, I_{ph} is light-generated photon current of the PV cell, v is the output voltage of the cell, R_s and R_{sh} are the series and parallel resistances of the PV cell, respectively, I_{sh} is the current through R_{sh}, N_s is the number of series connected PV cells, N_p is the number of parallel connected PV cells, $k = 1.3806503 \times 10^{-23} J/K$ is the Boltzmann constant, $q = 1.60217646 \times 10^{-19} C$ is the charge on electron, T is temperature in kelvin and A is the ideality factor of the diode. Note that, $R_{sh} >> R_s$.

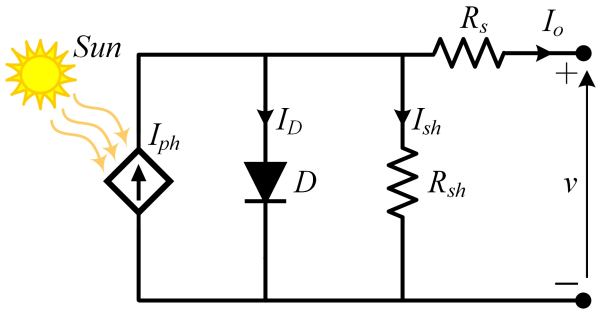

Figure 2. Single-diode equivalent model of a PV cell.

3.2. Dynamic model of the sound system

The main component of a sound system is the speaker, which is basically an electromechanical device. It is a dynamic load, equivalent to a permanent magnet DC (PMDC) motor. The dynamics of a speaker are described by the following second-order differential equation:

$$m\frac{d^2x}{dt^2} = K_f i_s - kx \tag{2}$$

In (2), the total mass of the diaphragm and coil is represented by m (kg), the displacement of the diaphragm by x, the spring constant by k (N/m) and magnetic force by $F = K_f i_s$. Where i_s denotes the input current to speaker (A) and K_f is the proportionality constant (N/A). The equivalent electric circuit of speaker is shown in Figure 3. Applying Kirchhoff's voltage law, the voltage input to speaker, v_s, can be expressed as follows:

$$v_s = L_s\frac{di_s}{dt} + R_s i_s + v_b \tag{3}$$

Where L_s and R_s represent the inductance (H) and resistance (Ω) of the speaker coil, respectively, $v_b = K_e\ (dx/dt) = K_e\omega$, v_b is the back emf (V), K_e is the back emf constant $(V.s/m)$ and ω is the velocity of the diaphragm (m/s).

In compact vector-matrix form, the dynamic state-space model of the speaker can be given as follows:

$$\begin{bmatrix} \frac{dx}{dt} \\ \frac{d\omega}{dt} \\ \frac{di_s}{dt} \end{bmatrix} = \begin{bmatrix} 0 & 1 & 0 \\ \frac{-k}{m} & 0 & \frac{K_f}{m} \\ 0 & -\frac{K_e}{L_s} & -\frac{R_s}{L_s} \end{bmatrix} \begin{bmatrix} x \\ \omega \\ i_s \end{bmatrix} + \begin{bmatrix} 0 \\ 0 \\ \frac{v_s}{L_s} \end{bmatrix} \tag{4}$$

3.3. DC-DC converter modelling

In this article, a noninverting topology of the buck-boost DC-DC converter [18] is employed as an interfacing stage between the source (PV array) and the dynamic load (speaker). The PV array output voltage, v_{pv}, is stepped up or stepped down to the desired voltage level, V_{MPP}, for achieving MPPT. This is accomplished by constantly varying the duty ratio, D, of the converter through the proposed nonlinear robust backstepping MPPT controller. The equivalent circuit diagram of the converter is shown in Figure 3.

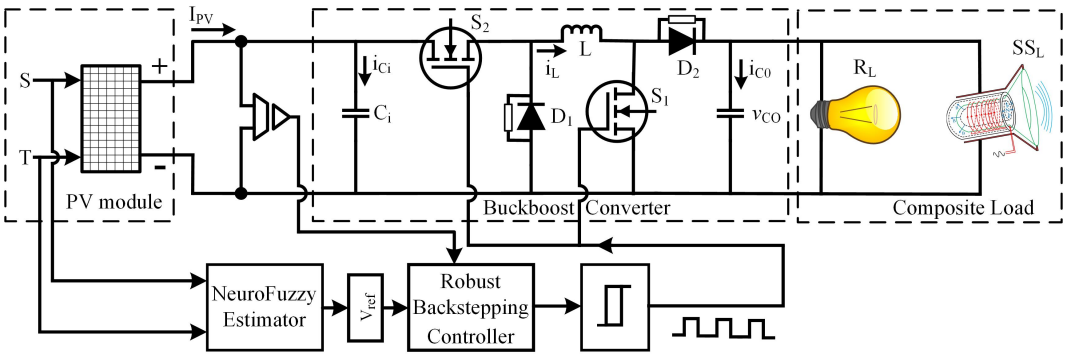

Figure 3. Proposed control system.

Generally, the converter can be operated in 2 different states. In State 1: both the controlled switches S_1 and S_2 are ON, while both the diodes D_1 and D_2 are reverse-biased. In State 2: both the switches S_1 and S_2 are OFF, while both the diodes D_1 and D_2 are forward-biased. For simplicity, the converter circuit is assumed to be operated in the continuous conduction mode (CCM), with ideal switches and diodes in the circuit. The voltage transfer function of the noninverting buck-boost DC-DC converter is given as follows:

$$\frac{v_{C_0}}{v_{C_i}} = \frac{D}{1-D} \tag{5}$$

In (5), $v_{C_i} = v_{pv}$ and $v_{C_0} = v$ (input voltage to dynamic load i.e. speaker). For the proposed controller design, average model of the converter over one switching period is considered. Hence, the state-space model of the converter based on inductor volt-second balance and capacitor charge balance principles is given as follows:

$$\begin{bmatrix} \frac{d\bar{v}_{pv}}{dt} \\ \frac{d\bar{i}_L}{dt} \\ \frac{d\bar{v}_{C_0}}{dt} \\ \frac{d\bar{i}_s}{dt} \end{bmatrix} = \begin{bmatrix} 0 & -\frac{D}{C_i} & 0 & 0 \\ \frac{D}{L} & 0 & \frac{D-1}{L} & 0 \\ 0 & \frac{1-D}{C_0} & -\frac{1}{RC_0} & -\frac{1}{C_0} \\ 0 & 0 & \frac{1}{L_s} & -\frac{R_s}{L_s} \end{bmatrix} \begin{bmatrix} \bar{v}_{pv} \\ \bar{i}_L \\ \bar{v}_{C_0} \\ \bar{i}_s \end{bmatrix} + \begin{bmatrix} \frac{i_{pv}}{C_i} \\ 0 \\ 0 \\ -\frac{v_b}{L_s} \end{bmatrix} \tag{6}$$

3.4. Average state-space modelling of the entire system

The average state-space model of the entire system consisting of the PV array, the DC-DC converter, and the dynamic load in compact vector-matrix form can be given as follows:

$$\begin{bmatrix} \frac{d\bar{v}_{pv}}{dt} \\ \frac{d\bar{i}_L}{dt} \\ \frac{d\bar{v}_{C_0}}{dt} \\ \frac{d\bar{i}_s}{dt} \\ \frac{d\bar{\omega}}{dt} \\ \frac{d\bar{x}}{dt} \end{bmatrix} = \begin{bmatrix} 0 & -\frac{D}{C_i} & 0 & 0 & 0 & 0 \\ \frac{D}{L} & 0 & \frac{D-1}{L} & 0 & 0 & 0 \\ 0 & \frac{1-D}{C_0} & -\frac{1}{RC_0} & -\frac{1}{C_0} & 0 & 0 \\ 0 & 0 & \frac{1}{L_s} & -\frac{R_s}{L_s} & 0 & 0 \\ 0 & 0 & 0 & \frac{k_f}{m} & 0 & -\frac{k}{m} \\ 0 & 0 & 0 & 0 & 1 & 0 \end{bmatrix} \begin{bmatrix} \bar{v}_{pv} \\ \bar{i}_L \\ \bar{v}_{C_0} \\ \bar{i}_s \\ \bar{\omega} \\ \bar{x} \end{bmatrix} + \begin{bmatrix} \frac{i_{pv}}{C_i} \\ 0 \\ 0 \\ -\frac{v_b}{L_s} \\ 0 \\ 0 \end{bmatrix} \tag{7}$$

where $\bar{v}_{pv}$, $\bar{i}_L$, $\bar{v}_{C_0}$, $\bar{i}_s$, $\bar{\omega}$ and $\bar{x}$ represents the average values of v_{pv}, i_L, v_{C_0}, i_s, ω and x, respectively.

4. Proposed control system design

The average-state space model of the entire system, described in (7) in compact vector-matrix form, can be transformed into a set of the following first-order differential equations:

$$\frac{d\bar{v}_{pv}}{dt} = \frac{1}{C_i}\left(I_{pv} - D\bar{i}_L\right) \tag{8}$$

$$\frac{d\bar{i}_L}{dt} = \frac{1}{L}\left(D\bar{v}_{pv} + \bar{v}_{C_0}(D-1)\right) \tag{9}$$

$$\frac{d\bar{v}_{C_0}}{dt} = \frac{1}{C_0}\left(\bar{i}_L - \frac{\bar{v}_{C_0}}{R} - \bar{i}_s - D\bar{i}_L\right) \tag{10}$$

$$\frac{d\bar{i}_s}{dt} = \frac{1}{L_s}\left(\bar{v}_{C_0} - \bar{i}_s R_s - v_b\right) \tag{11}$$

$$\frac{d\bar{\omega}}{dt} = \frac{1}{m}\left(k_f\bar{i}_s - k\bar{x}\right) \tag{12}$$

$$\frac{d\bar{x}}{dt} = \bar{\omega} \tag{13}$$

4.1. Robust backstepping based MPPT controller design

In this section a robust backstepping based MPPT controller is designed for the noninverting buck-boost DC-DC converter described in (8)-(13). The closed-loop control system is shown in Figure 3. The block (NeuroFuzzy estimator) estimates the online reference peak power voltage, v_{ref} for cell temperature, T, and solar irradiation, S. The block (robust backstepping controller) uses the estimated value v_{ref} as a set point to control the duty ratio, D, and let the converter input voltage $\bar{v}_{pv}$ to track v_{ref}.

To develop the robust backstepping MPPT technique and stabilize the noninverting buck-boost converter to the origin (zero error), the first tracking error Σ_1 is defined to impose buck-boost input voltage, v_{pv}, to track the reference peak power voltage V_{MPP} or v_{ref} (with zero tracking error). That is,

$$\Sigma_1 = \bar{v}_{pv} - v_{ref} \tag{14}$$

The objective is to converge the error signal Σ_1 to zero. Taking derivative of (14) w.r.t time gives,

$$\dot{\Sigma}_1 = \dot{\bar{v}}_{pv} - \dot{v}_{ref} \tag{15}$$

Inserting $\dot{\bar{v}}_{pv}$, from (8) in (15), gives the following expression:

$$\dot{\Sigma}_1 = \frac{I_{pv}}{C_i} - D\frac{\bar{i}_L}{C_i} - \dot{v}_{ref} \tag{16}$$

In (16) taking $\bar{i}_L$ a virtual control input and let V_1 be a positive definite Lyapunov candidate function for checking the convergence of Σ_1 to 0.

$$V_1 = \frac{1}{2}\Sigma_1^2 \tag{17}$$

In order to assure the asymptotic stability, the Lyapunov function must be positive definite and radially unbounded and its derivative with respect to time must be negative definite. Now, taking the time derivative of (17) gives the following expression:

$$\dot{V}_1 = \Sigma_1\dot{\Sigma}_1 \tag{18}$$

Using value of $\dot{\Sigma}_1$ from (16) in (18)

$$\dot{V}_1 = \Sigma_1\left(\frac{I_{pv}}{C_i} - D\frac{\bar{i}_L}{C_i} - \dot{v}_{ref}\right) \tag{19}$$

To introduce robustness into the backstepping strategy, $\bar{i}_L$ becomes as follows:

$$i_{Lref} = \left(\frac{I_{pv}}{C_i} - \dot{v}_{ref} + k_1 e_1 + k_2 sign\left(e_1\right)\right)\frac{C_i}{D} \tag{20}$$

where k_1 and k_2 must be positive constants. With this choice of $\bar{i}_L$, (19) takes the following form:

$$\dot{V}_1 = -k_1\Sigma_1^2 - k_2\Sigma_1 sign\left(\Sigma_1\right) \tag{21}$$

Now, treating i_{Lref} as a new reference for the next step which will be tracked by the second state of the system. The tracking error is defined as follows:

$$\Sigma_2 = \bar{i}_L - i_{Lref} \tag{22}$$

and

$$\bar{i}_L = \Sigma_2 + i_{Lref} \tag{23}$$

Putting (23) in (19), one may get

$$\dot{V}_1 = \Sigma_1 \left(\frac{I_{pv}}{C_i} - D \left(\frac{\Sigma_2 + i_{Lref}}{C_i} \right) - \dot{v}_{ref} \right) \tag{24}$$

$$= \Sigma_1 \left(\frac{I_{pv}}{C_i} - D \frac{i_{Lref}}{C_i} - \dot{v}_{ref} - D \frac{\Sigma_2}{C_i} \right)$$

Substituting (20) in the above expression, one has

$$\dot{V}_1 = -k_1 \Sigma_1^2 - k_2 \Sigma_1 sign\left(\Sigma_1\right) - D \frac{\Sigma_2 \Sigma_1}{C_i} \tag{25}$$

This inequality can also be written as follows:

$$\dot{V}_1 = -2k_1 V_1 - \sqrt{2} k_2 \sqrt{V_1} - D \frac{\Sigma_2 \Sigma_1}{C_i} \tag{26}$$

Now, differentiating (22) with respect to time, it becomes as follows:

$$\dot{\Sigma}_2 = \dot{\bar{i}}_L - \dot{i}_{Lref} \tag{27}$$

where the time derivative of i_{Lref} ($\dot{i}_{Lref}$)is calculated as follows:

$$\dot{i}_{Lref} = \frac{1}{D^2} \left[(D) \left(\dot{I}_{pv} - C_i \ddot{v}_{ref} + k_1 C_i \dot{\Sigma}_1 \right) - \left(I_{pv} - C_i \dot{v}_{ref} + k_1 C_i \Sigma_1 + k_2 C_i sign\left(\Sigma_1\right) \right) \left(\dot{D} \right) \right] \tag{28}$$

Carrying out some algebraic simplification, the expression of $\dot{i}_{Lref}$ becomes as follows:

$$\dot{i}_{Lref} = \frac{1}{D} \left[\dot{I}_{pv} - C_i \ddot{v}_{ref} - C_i k_1^2 \Sigma_1 - C_i k_1 k_2 sign\left(\Sigma_1\right) \right] - k_1 \Sigma_2 - \frac{\dot{D}}{D} i_{Lref} \tag{29}$$

Using it in (27), one has

$$\dot{\Sigma}_2 = \dot{\bar{i}}_L - \left[\left(\frac{1}{D} \right) \left(\dot{I}_{pv} - C_i \ddot{v}_{ref} - C_i k_1^2 \Sigma_1 - C_i k_1 k_2 sign\left(\Sigma_1\right) \right) - k_1 \Sigma_2 - \frac{\dot{D}}{D} i_{Lref} \right] \tag{30}$$

A composite Lyapunov function, V_c, is defined to ensure convergence of the errors Σ_1 and Σ_2 to zero and the asymptotic stability of the system, as follows:

$$V_c = V_1 + \frac{1}{2} \Sigma_2^2 \tag{31}$$

The time derivative of V_c along (25) becomes

$$\dot{V}_c = -k_1 \Sigma_1^2 - k_2 \Sigma_1 sign\left(\Sigma_1\right) + \Sigma_2 \left(\dot{\Sigma}_2 - D \frac{\Sigma_1}{C_i} \right) \tag{32}$$

For V_c to be negative definite, let

$$\dot{\Sigma}_2 - D\frac{\Sigma_1}{C_i} = -k_3\Sigma_2 - k_4 sign\left(\Sigma_2\right) \tag{33}$$

where k_3 and k_4 are positive constants. Using values of $\dot{\Sigma}_2$ from (30) and $\dot{\bar{i}}_L$ from (9) in (33), it gives

$$\begin{aligned} -k_3\Sigma_2 - k_4 sign\left(\Sigma_2\right) = &- D\frac{\Sigma_1}{C_i} + \left(\left(\frac{Dv_{pv}}{L}\right) + \left(\frac{D-1}{L}\right)v_{C_0}\right) - \left(\frac{1}{D}\right)\Big(\dot{I}_{pv} - C_i\ddot{v}_{ref} - C_i k_1^2\Sigma_1 \\ &- C_i k_1 k_2 sign\left(\Sigma_1\right)\Big) + k_1\Sigma_2 + \frac{\dot{D}}{D}i_{Lref} \end{aligned} \tag{34}$$

Solving for $\dot{D}$, one gets the final expression of the control law as follows

$$\begin{aligned} \dot{D} = &\frac{D}{i_{Lref}}\left[-k_3\Sigma_2 - k_4 sign(\Sigma_1) + D\frac{\Sigma_1}{C_i} - k_1\Sigma_2\right] - \frac{D}{i_{Lref}}\left[\left(\frac{D\bar{v}_{pv}}{L}\right) + \left(\frac{D-1}{L}\right)\bar{v}_{C_0}\right] + \frac{D}{i_{Lref}}\left[\left(\frac{1}{D}\right)\left(\dot{I}_{pv}\right.\right. \\ &\left.\left. - C_i\ddot{v}_{ref} - C_i k_1^2\Sigma_1 - C_i k_1 k_2 sign\left(\Sigma_1\right)\right)\right] \end{aligned} \tag{35}$$

A computational flowchart for implementation of the proposed MPPT control law is illustrated in Figure 4.

4.2. Stability of zero dynamics

Since, a 2 step robust backstepping law is designed, the dynamic equations (10)-(13) are straight-a-way the internal dynamics of the under consideration PV system accompanied by the sound system. According to the nonlinear theory [19], the zero dynamics can be obtained by substituting the applied control input, u, and the control driven states, $\bar{v}_{pv}$ and $\bar{i}_L$, equal to zero in the internal dynamics. Thus one has the following zero dynamics:

$$\begin{bmatrix} \frac{d\bar{v}_{C_0}}{dt} \\ \frac{d\bar{i}_s}{dt} \\ \frac{d\bar{\omega}}{dt} \\ \frac{d\bar{x}}{dt} \end{bmatrix} = \begin{bmatrix} -\frac{1}{RC_0} & -\frac{1}{C_0} & 0 & 0 \\ \frac{1}{L_S} & \frac{-R_s}{L_s} & 0 & 0 \\ 0 & \frac{k_f}{m} & 0 & -\frac{k}{m} \\ 0 & 0 & 1 & 0 \end{bmatrix} \begin{bmatrix} \bar{v}_{C_0} \\ \bar{i}_s \\ \bar{\omega} \\ \bar{x} \end{bmatrix} + \begin{bmatrix} 0 \\ \frac{-v_b}{L_s} \\ 0 \\ 0 \end{bmatrix} \tag{36}$$

This is a linear time invariant (LTI) nonhomogeneous system that can be represented, in general form, as follows:

$$\dot{\bar{x}} = \bar{A}\bar{x} + \bar{B} \tag{37}$$

where $\bar{x} = [\bar{v}_{c_0}, \bar{i}_s, \bar{\omega}, \bar{x}]^T$ represents zero dynamics states vector, $\bar{A}$ is the respective system distribution matrix, and $\bar{B}$ is a vector of time varying nonvanishing disturbances which depend on the back emf, v_b. This system has general solution of the following form:

$$\bar{x}(t) = e^{\bar{A}t}\bar{x}(0) + e^{\bar{A}t}\int_{t_0}^{t} e^{-r\bar{A}}\bar{B}dr \tag{38}$$

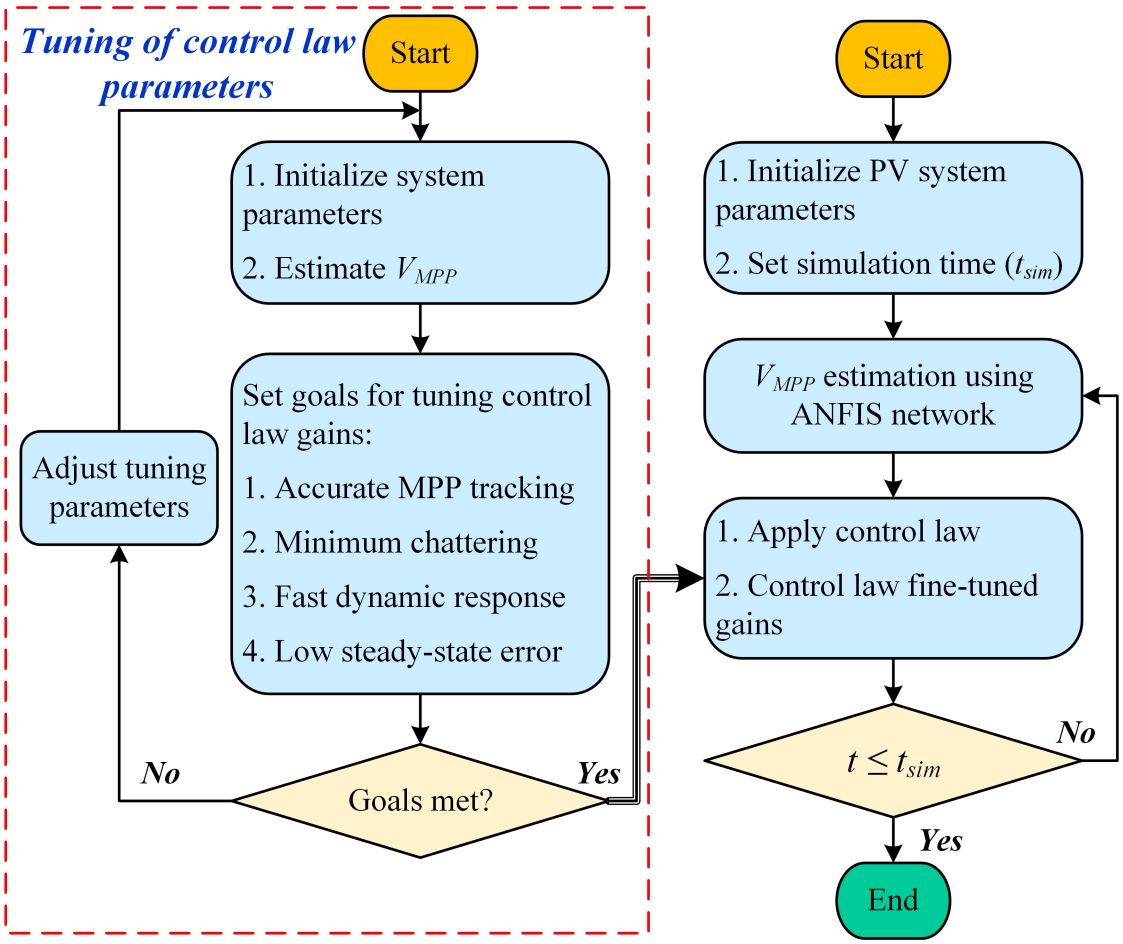

Figure 4. Computational flowchart for implementation of the proposed MPPT control law.

Since all the typical plant parameters are positive, the system (36) of zero dynamics has 2 poles on the $jw-axis$ i.e., at $\pm j-\frac{k}{m}$ and 2 poles in the left half plan (LHP) at $-\frac{R_sRC_0+L_s}{2RL_sC_0}\pm\frac{1}{2}\sqrt{(\frac{R_sRC_0+L_s}{2RL_sC_0})^2-8\frac{R}{RL_sC_0L_a}}$. Note that, as long as the discriminant in the square root remains negative, it will give rise to conjugate poles with negative real parts. Thus, the exponential term $e^{\bar{A}t}$, which can be calculated via Caylay-Hamilton approach on the spectrum of the above defined LHP poles, has 2 oscillatory modes and 2 modes with decaying oscillations. Based on the information of the poles, the overall response of the zero dynamics will initially observe decaying oscillatory response to the vicinity of the origin, and then all the states will remain ultimately bounded. In other words, this also confirms that initially the zero dynamics will show a minimum phase nature and, as the effects of the exponential terms die out, the over all zero dynamics will stay bounded in a small neighbourhood. This confirms the practical asymptotic convergence of the zero dynamics. Hence, the control will effectively track the reference in the presence of the practical asymptotic convergence of the internal dynamics. Now, in the forthcoming sections, the simulation results will demonstrate, the effectiveness of the proposed law in sound details.

5. Simulation results and discussion

Matlab/Simulink package has been used for carrying out simulations under varying atmospheric conditions and faults. The parameters of the PV array, DC-DC converter, speaker and proposed MMPT controller are described in Table 1. The performance of the proposed MPPT technique is tested under simultaneous variation in atmospheric conditions (temperature and irradiance), and against multiple faults occurring in the system.

Table 1. Parameters of the PV system

Type	Name of Parameter	Symbol	Magnitude
PV Array	Maximum power per module	P_{max}	$1,555\ W$ @ Standard Test Conditions
	Number of Cells per module	N_s	72
	Voltage at maximum power per module	V_{mp}	$102.60\ V$
	Open circuit voltage per module	V_{oc}	$165.80\ V$
	Short circuit current per module	I_{sc}	$17.56\ A$
	Current at maximum power per module	I_{mp}	$15.16\ A$
	Number of PV modules per string	...	4
	Number of PV modules per array	...	16
	Total power output of PV array	...	$24,880\ W$
Converter	Input Capacitor	C_i	$1 \times 10^{-3}\ F$
	Inductor	L	$20 \times 10^{-3}\ H$
	Output capacitor	C_0	$48 \times 10^{-3}\ F$
	Load resistance	R_L	$50\ \Omega$
	IGBT switching frequency	f_s	$5{,}000\ Hz$
Speaker	Back emf constant	k_e	15
	Speaker resistance	R_s	$10\ \Omega$
	Speaker inductance	L_s	$10^{-3}\ H$
	Proportionality constant	k_f	15 N/A
	Spring constant	k	$5 \times 10^5\ N/m$
	Spring and diaphragm mass	m	$0.001\ kg$
Controller	Constant	k_1	60
	Constant	k_2	10
	Constant	k_3	5,000
	Constant	k_4	10

5.1. Comparison of the proposed MPPTtechnique with backstepping and integral backstepping based MPPT techniques

In this section, the performance of the proposed technique is tested under simultaneous variation of temperature and irradiance, and faults occurring in the system and then compared with backstepping [10] and integral backstepping [11] based MPPT techniques. The temperature and irradiance are varied under rapid successions, that is, ($25\,^oC$, $65\,^oC$, and $25\,^oC$) and ($650\,W/m^2$, $1000\,W/m^2$ and $650\,W/m^2$), respectively. The duration of each succession is kept 0.1 s. Furthermore, time varying sinusoidal faults, that is, $9000usin(t)/C_i$ (during

the time interval 0.6 s to 0.8 s) and $0.5usin(t)/C_i$ (during the time interval of 0.16 s to 0.18 s) are injected into $\bar{v}_{C_0}$ and $\bar{i}_L$, respectively.

Figures 5 and 6 demonstrate the PV array power-voltage and current-voltage characteristics and the MPPs, respectively, under varying meteorological conditions and faults. Where,

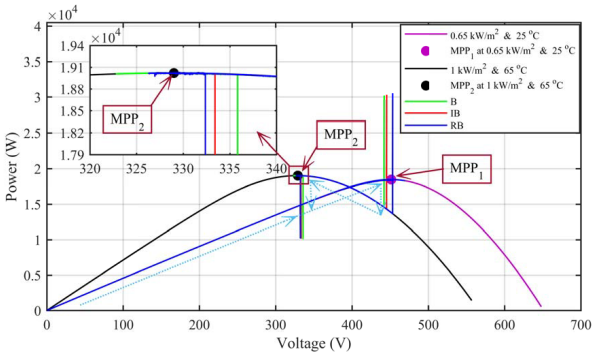

Figure 5. Power-voltage characteristic curves of the PV array under varying atmospheric conditions and multiple faults.

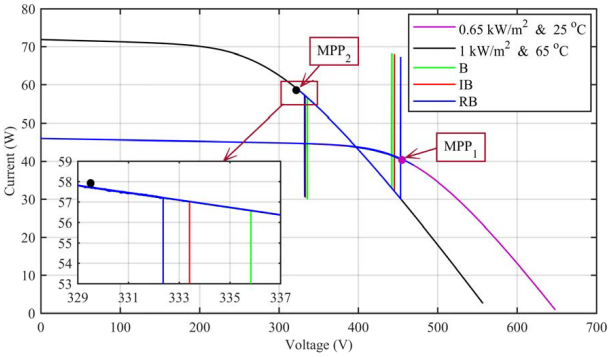

Figure 6. Current-voltage characteristic curves of the PV array under varying atmospheric conditions and multiple faults.

$at\ MPP_1:\ (S = 650\ W/m^2,\ T = 25\ ^0C,\ V_{MPP} = 451.516\ V,\ I_{MPP} = 40.929\ A,\ P_{MPP} = 1.846 \times 10^4$ W), and $at\ MPP_2:\ (S = 1000\ W/m^2,\ T = 65\ ^0C,\ V_{MPP} = 329\ V,\ I_{MPP} = 57.821\ A,\ P_{MPP} = 1.902 \times 10^4\ W)$.

From these figures, it can be clearly seen that the proposed scheme tracks the MPP better than the existing backstepping and integral backstepping techniques. The PV array output voltage comparison is depicted in Figure 7, under different MPPT candidates. Where, in Figure 7(a), the proposed control scheme shows the better transient response, in terms of the fastest rise time and the fastest settling time, under the meteorological changes as compared to the existing MPPT techniques. Similarly, the maximum steady-state error can be seen in the backstepping based MPPT controller as depicted in Figure 7(b). The PV array output voltage deviates from V_{ref}, due to occurrence of faults in the system, as shown in Figure 7(c). However, the proposed control approach achieves the steady-state faster (in about $t = 0.005\ s$), which is the minimum response time to faults occurring in the system, as compared to the backstepping and integral backstepping control schemes. The proposed scheme deviates the least (from $V_{ref} = 329\ V$ to $416\ V$), as compared to the backstepping (from $329\ V$ to $453\ V$) and integral backstepping (from $329\ V$ to $442\ V$). Similarly, as shown in Figure 8, the proposed technique extracts the maximum power from the PV array with minimum deviation under faults than its other two contenders. From Figures 7 and 8, it can easily be concluded that the proposed technique deviates the least under faults and then recovers and settles earlier than the backstepping and integral backstepping techniques. Figure 9 represents various performance indices (IAE, ITAE, ISE and ITSE) [20]. Based on these performance indices, it can be deduced that the proposed technique outperforms the backstepping and integral backstepping techniques in terms of providing the minimum accumulative error and achieving the best MPPT performance. Figure 10 demonstrates the efficiency comparison of the PV array under different MPPT candidates. It is evident that the proposed technique transfers the maximum power from the PV array to the dynamic load, while achieving the highest efficiency of around 97%, as compared to other 2 MPPT candidates.

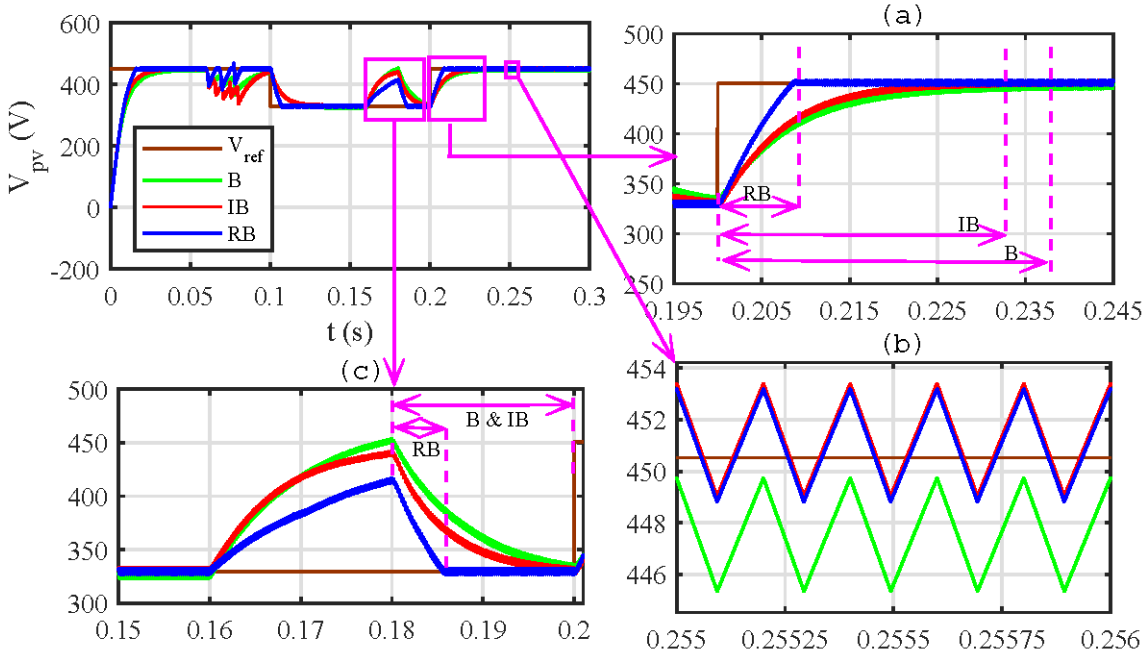

Figure 7. PV array output voltages comparison under different atmospheric conditions and multiple faults.

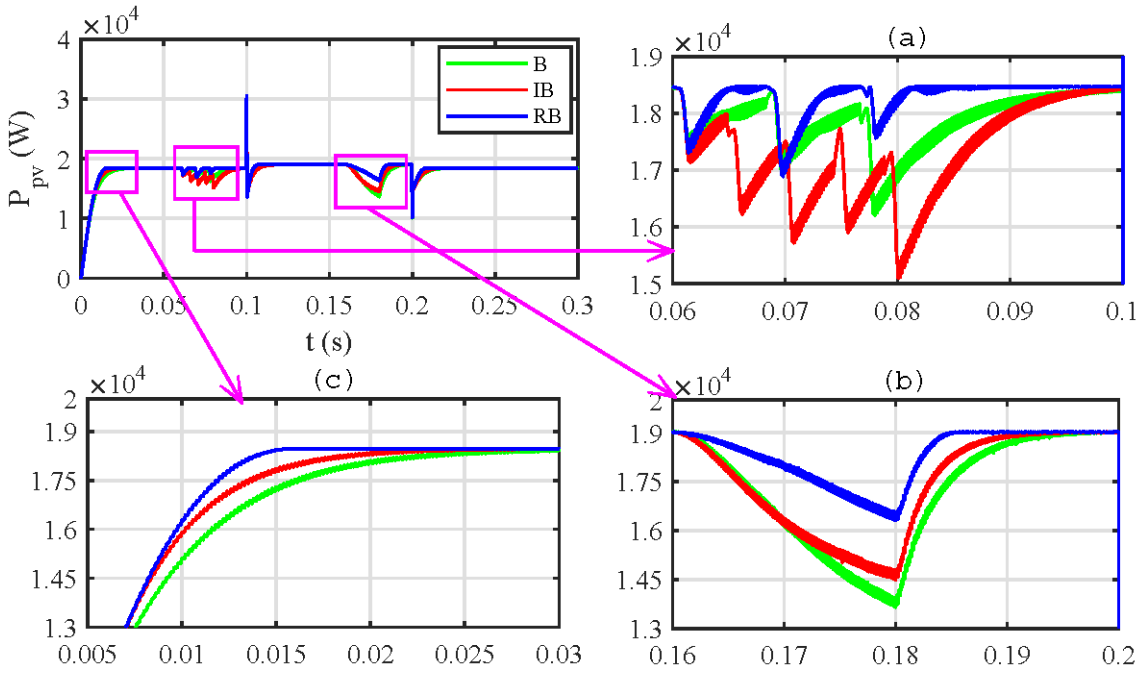

Figure 8. PV array output power comparison under varying atmospheric conditions and multiple faults.

5.2. Comparison of the proposed MPPT technique with traditional MPPT techniques

In this section, the performance of the proposed technique is tested under the same conditions, described in the previous section, and then compared with the traditional PID and P&O based MPPT techniques. Figure 11,

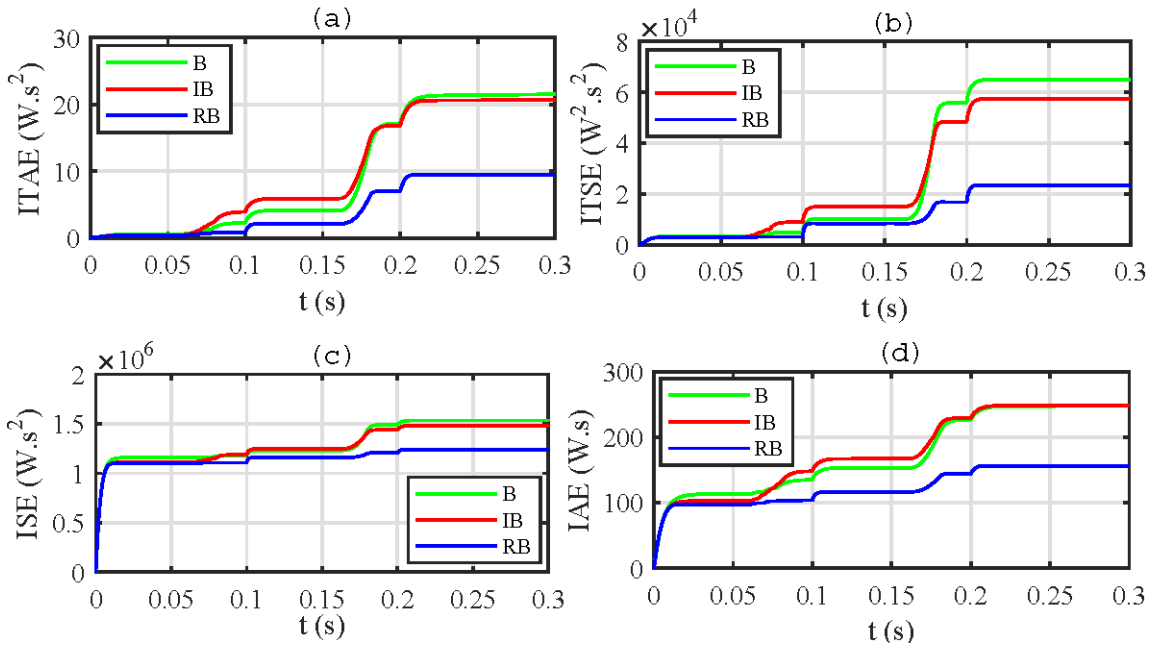

Figure 9. Performance indices comparison of the PV array under varying atmospheric conditions and multiple faults.

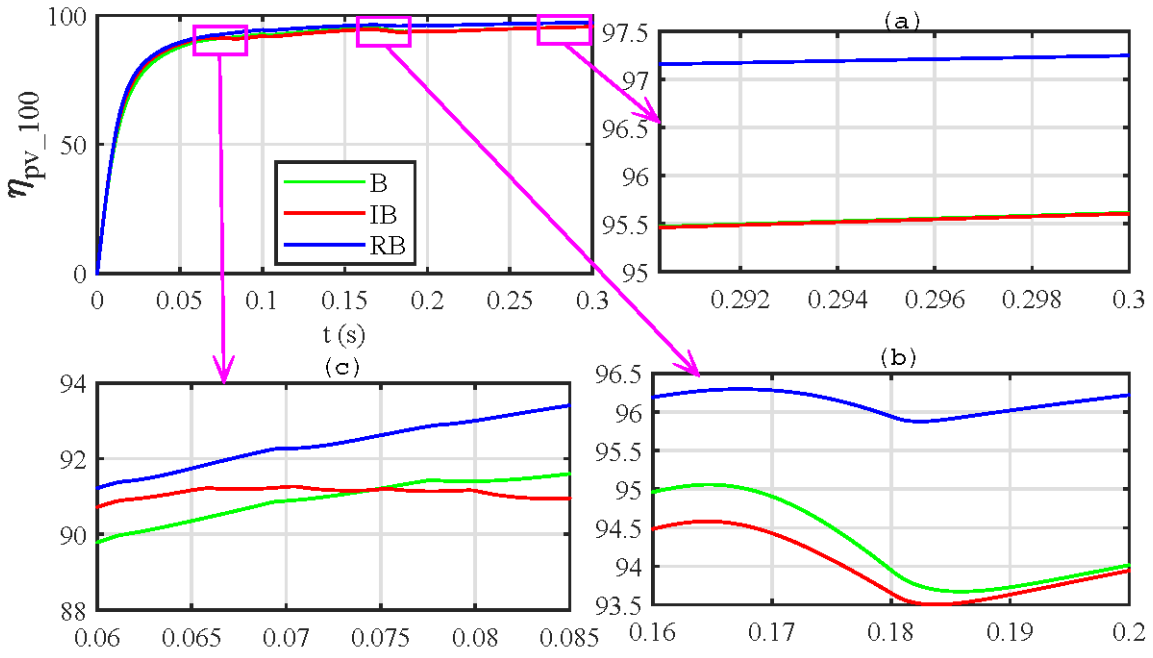

Figure 10. PV array efficiency comparison under varying atmospheric conditions and multiple faults.

shows the PV array output powers for the 3 techniques. It is evident that both the PID and P&O techniques exhibit larger oscillations in powers. On the other hand, the proposed technique shows smaller variations in power, thus outperforming the conventional MPPT techniques.

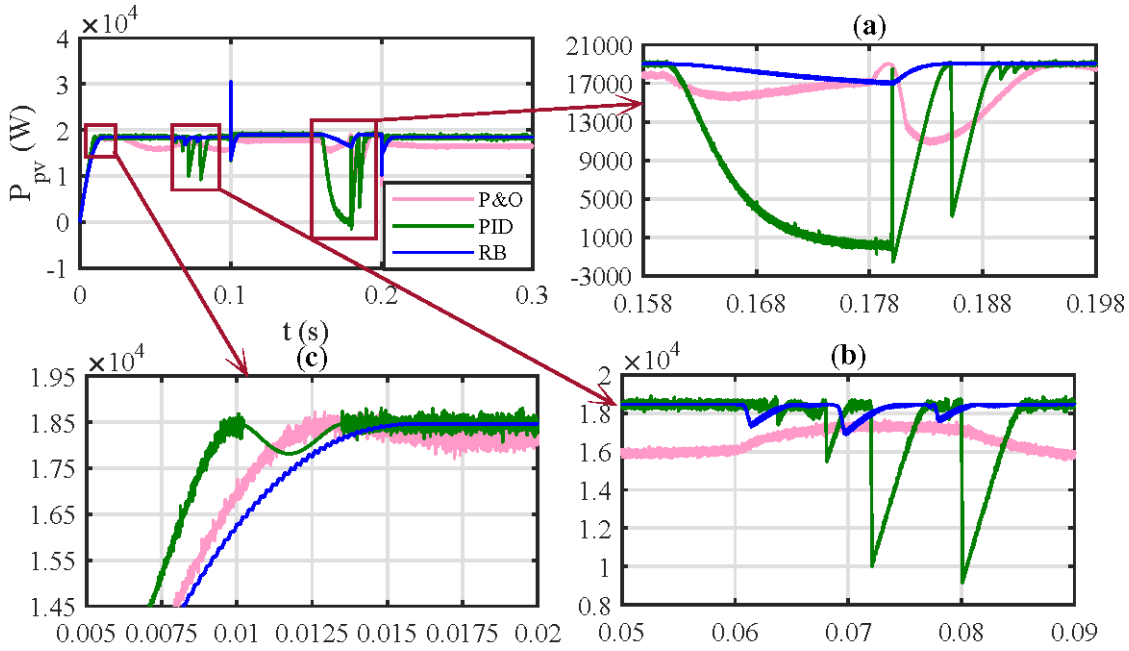

Figure 11. PV array output power comparison under varying atmospheric conditions and multiple faults.

6. Conclusion

In this research article, a new nonlinear robust backstepping-based MPPT technique has been proposed for a standalone PV array connected to a dynamic load (speaker) and its performance comparison with existingbackstepping, integral backstepping and traditional PID and P&O based MPPT techniques is provided. Simulations, performed in Matlab/Simulink package, verify the effectiveness of the proposed MPPT technique and demonstrate its superior performance to the backstepping, integral backstepping and conventional MPPT techniques under simultaneous variation in irradiance and temperature and multiple faults occurring in the system. The proposed technique is not only robust against faults and varying atmospheric conditions, but also outperforms other techniques in terms of tracking, efficiency, and various performance indices.

References

[1] Mohanty M, Selvakumar S, Koodalsamy C, Simon SP. Global maximum operating point tracking for PV system using fast convergence firefly algorithm. Turkish Journal of Electrical Engineering and Computer Science 2019; 27(6): 4640-4658. doi: 10.3906/elk-1805-108

[2] Nagarani B, Nesmony J. Performance enhancement of photovoltaic system using genetic algorithm-based maximum power point tracking. Turkish Journal of Electrical Engineering and Computer Science 2019; 27(4): 3015-3025. doi: 10.3906/elk-1801-189

[3] Subudhi B, Pradhan R. A comparative study on maximum power point tracking techniques for photovoltaic power systems. IEEE Trans. Sustainable Energy 2012; 4(1): 89-98. doi: 10.1109/TSTE.2012.2202294

[4] Roy TK, Mahmud MA, Oo AMT, Bansal R, Haque ME. Nonlinear Adaptive Backstepping Controller Design for Three-Phase Grid-Connected Solar Photovoltaic Systems. Electric Power Components and Systems 2017; 45(20): 2275-2292. doi: 10.1080/15325008.2018.1431334

[5] Kim, Il-Song. Sliding mode controller for the single-phase grid-connected photovoltaic system. Applied Energy 2006; 83(10): 1101-1115. doi: 10.1016/j.apenergy.2005.11.004

[6] Mahmud MA, Pota HR, Hossain MJ, Roy NK. Robust partial feedback linearizing stabilization scheme for three-phase grid-connected photovoltaic systems. IEEE J. Photovoltaics 2013; 4(1): 423-431. doi: 10.1109/JPHOTOV.2013.2281721

[7] Kotsopoulos A, Duarte JL, Hendrix MAM. Predictive DC voltage control of single-phase PV inverters with small DC link capacitance. In 2003 IEEE International Symposium on Industrial Electronics (Cat. No. 03TH8692); Rio de Janeiro, Brazil; 2003. pp. 793-797. doi: 10.1109/ISIE.2003.1267921.

[8] Fadili AE, Giri F, Magri AE. Reference voltage optimizer for maximum power point tracking in triphase grid-connected photovoltaic systems. International Journal of Electrical Power & Energy Systems 2014; 60: 293-301. doi: 10.1016/j.ijepes.2014.03.029

[9] Kim IS. Robust maximum power point tracker using sliding mode controller for the three-phase grid-connected photovoltaic system. Solar Energy 2007; 81(3): 405-414. doi: 10.1016/j.solener.2006.04.005

[10] Naghmash, Armghan H, Ahmad I, Armghan A, Khan S, Arsalan M. Backstepping based non-linear control for maximum power point tracking in photovoltaic system. Solar Energy 2018; 159: 134-141. doi: 10.1016/j.solener.2017.10.062

[11] Arsalan M, Iftikhar R, Ahmad I, Hasan A, Sabahat K, Javeria A. MPPT for photovoltaic system using nonlinear backstepping controller with integral action. Solar Energy 2018; 170: 192-200. doi: 10.1016/j.solener.2018.04.061

[12] Wang J, Bo D, Ma X, Zhang Y, Li Z, Miao Q. Adaptive back-stepping control for a permanent magnet synchronous generator wind energy conversion system. International Journal of Hydrogen Energy 2019; 44(5): 3240-3249. doi: 10.1016/j.ijhydene.2018.12.023

[13] Krstic M, Kanellakopoulos I, Kokotović PV. Nonlinear and adaptive control design. John Wiley & Sons Inc., 1995.

[14] Errami Y, Obbadi A, Sahnoun S, Benhmida M, Ouassaid M, Maaroufi M. Design of a nonlinear backstepping control strategy of grid interconnected wind power system based PMSG. AIP Conference Proceedings, pp. 030053, 2016. doi: 10.1063/1.4959449

[15] Krstic M, Smyshlyaev A. Boundary control of PDEs: A course on backstepping designs. Society for Industrial and Applied Mathematics, Philadelphia, Pennsylvania, United States, 2008.

[16] Hassan, Syed Zulqadar, Hui Li, Tariq Kamal, Uğur Arifoğlu, Sidra Mumtaz, and Laiq Khan. Neuro-fuzzy wavelet based adaptive MPPT algorithm for photovoltaic systems. Energies 2017; 10(3): 394. doi: 10.3390/en10030394

[17] Harrag A, Messalti S. Variable step size modified P&O MPPT algorithm using GA-based hybrid offline/online PID controller. Renewable Sustainable Energy Reviews 2015; 49: 1247-1260. doi: 10.1016/j.rser.2015.05.003

[18] Erickson RW, Maksimovic D. Fundamentals of power electronics. New York, US: Springer, 2001. doi: 10.1007/b100747

[19] Isidori A. Nonlinear control systems. London, UK: Springer-Verlag, 1993. doi: 10.1007/978-1-84628-615-5

[20] Duman S, Yörükeren N, Altaş İH. Gravitational search algorithm for determining controller parameters in an automatic voltage regulator system. Turkish Journal of Electrical Engineering and Computer Science 2016; 24(4): 2387-2400. doi: 10.3906/elk-1404-14